LETTER

Corrected: Publisher Correction

https://doi.org/10.1038/s41586-019-1096-4

No detection of methane on Mars from early ExoMars Trace Gas Orbiter observations

Oleg Korablev[1]*, Ann Carine Vandaele[2], Franck Montmessin[3], Anna A. Fedorova[1], Alexander Trokhimovskiy[1], François Forget[4], Franck Lefèvre[3], Frank Daerden[2], Ian R. Thomas[2], Loïc Trompet[2], Justin T. Erwin[2], Shohei Aoki[2], Séverine Robert[2], Lori Neary[2], Sébastien Viscardy[2], Alexey V. Grigoriev[1], Nikolay I. Ignatiev[1], Alexey Shakun[1], Andrey Patrakeev[1], Denis A. Belyaev[1], Jean-Loup Bertaux[1,3], Kevin S. Olsen[3], Lucio Baggio[3], Juan Alday[5], Yuriy S. Ivanov[6], Bojan Ristic[2], Jon Mason[7], Yannick Willame[2], Cédric Depiesse[2], Laszlo Hetey[2], Sophie Berkenbosch[2], Roland Clairquin[2], Claudio Queirolo[2], Bram Beeckman[2], Eddy Neefs[2], Manish R. Patel[7], Giancarlo Bellucci[8], Jose-Juan López-Moreno[9], Colin F. Wilson[5], Giuseppe Etiope[8,10,11], Lev Zelenyi[1], Håkan Svedhem[12], Jorge L. Vago[12] & The ACS & NOMAD Team[13]

The detection of methane on Mars has been interpreted as indicating that geochemical or biotic activities could persist on Mars today[1]. A number of different measurements of methane show evidence of transient, locally elevated methane concentrations and seasonal variations in background methane concentrations[2–5]. These measurements, however, are difficult to reconcile with our current understanding of the chemistry and physics of the Martian atmosphere[6,7], which—given methane's lifetime of several centuries—predicts an even, well mixed distribution of methane[1,6,8]. Here we report highly sensitive measurements of the atmosphere of Mars in an attempt to detect methane, using the ACS and NOMAD instruments onboard the ESA-Roscosmos ExoMars Trace Gas Orbiter from April to August 2018. We did not detect any methane over a range of latitudes in both hemispheres, obtaining an upper limit for methane of about 0.05 parts per billion by volume, which is 10 to 100 times lower than previously reported positive detections[2,4]. We suggest that reconciliation between the present findings and the background methane concentrations found in the Gale crater[4] would require an unknown process that can rapidly remove or sequester methane from the lower atmosphere before it spreads globally.

The first positive detections of methane on Mars were published in 2004 from the analysis of 1999 ground-based spectroscopic observations[9], and from the Planetary Fourier Spectrometer (PFS) instrument on board the European Space Agency (ESA)'s Mars Express orbiter[10]. Mixing ratios for methane of about 10 parts per billion by volume (p.p.b.v.) were reported. This stirred up excitement in the scientific community, but both observations were at the limit of the instrumental sensitivity. Another set of ground-based echelle-spectroscopy observations reported a plume of methane developed over 60 northern summer sols (Martian solar days)[2] in 2003, reaching a peak value of 45 ± 10 p.p.b.v. No or little methane (≤7–8 p.p.b.v.) was detected before and after this event[2,11]. One more ground-based detection of 10 p.p.b.v. was reported in 2005[12]. Starting from October 2012 the Tunable Laser Spectrometer (TLS) of the Sample Analysis at Mars (SAM) instrument onboard NASA's Curiosity rover (MSL, Mars Science Laboratory) performed local samplings of Mars's atmosphere in the Gale crater. The readings first remained below 2–3 p.p.b.v., yet were followed by a number of positive detections in 2013–2017, the most notable of which was 9 p.p.b.v. in January 2014[3]. This result was questioned in ref. [13] on the basis of potential rover self-contamination, an argument later rejected by the TLS team, who showed that such a hypothesis could be excluded[4]. A TLS detection of 5.8 p.p.b.v. in 2013[4] has been independently confirmed by Planetary Fourier Spectrometer target observation of the surroundings of Gale crater, resulting in a value of 15.5 p.p.b.v. (ref. [5]). More sensitive TLS samplings led to the discovery of a seasonally varying 'background level' ranging[4] between 0.24 and 0.65 p.p.b.v.

In the oxidizing Martian atmosphere, methane is slowly destroyed by ultraviolet photolysis and reactions with OH and O(^{1}D), where D is deuterium. Our current understanding of Mars photochemistry suggests that methane should have a lifetime[1,6,8] of 250–300 years. Therefore, its detection, even in small quantities, requires sustained replenishment. Methane on Mars has attracted much interest because on Earth, most of the atmospheric methane has a biological origin. Thus, the Martian atmospheric methane might hint at active or extant microbial life or at the existence of organic matter. However, methane can also be formed abiotically, by low-temperature chemical reactions (for example, CO_2 hydrogenation) or magmatic processes[14,15].

Given its potential implications for exobiology or geochemistry, highly sensitive measurements of atmospheric methane and other trace species were identified as the primary science goal of the ESA-Roscosmos ExoMars Trace Gas Orbiter (TGO) mission[16]. The two-hour circular orbit of the TGO satellite was designed to detect

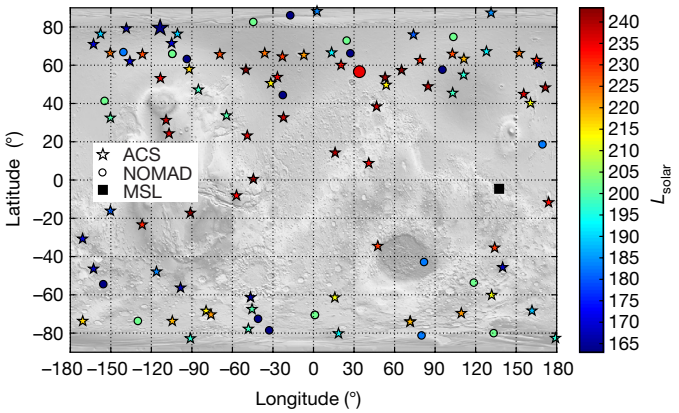

Fig. 1 | Map of ExoMars TGO methane measurements by ACS (stars) and NOMAD (circles) used in this study. The symbols corresponding to example measurements considered in this study are enlarged. The colour scale denotes L_{solar} (the areocentric solar longitude). Gale crater (the location of the Curiosity rover) is marked by a black square.

[1]Space Research Institute (IKI), Russian Academy of Sciences (RAS), Moscow, Russia. [2]Royal Belgian Institute for Space Aeronomy (BIRA-IASB), Brussels, Belgium. [3]Laboratoire Atmosphères, Milieux, Observations Spatiales (LATMOS), UVSQ Université Paris-Saclay, Sorbonne Université, CNRS, Paris, France. [4]Laboratoire de Météorologie Dynamique (LMD), CNRS Jussieu, Paris, France. [5]Department of Physics, Oxford University, Oxford, UK. [6]Main Astronomical Observatory (MAO), National Academy of Sciences of Ukraine, Kiev, Ukraine. [7]School of Physical Sciences, The Open University, Milton Keynes, UK. [8]Instituto de Astrofisica e Planetologia Spaziali, INAF, Rome, Italy. [9]Instituto de Astrofisica de Andalucía, Consejo Superior de Investigaciones Científicas (CSIC), Granada, Spain. [10]Istituto Nazionale di Geofisica e Vulcanologia, Rome, Italy. [11]Faculty of Environmental Science and Engineering, Babes-Bolyai University, Cluj-Napoca, Romania. [12]European Space Research and Technology Centre (ESTEC), ESA, Noordwijk, The Netherlands. [13]A list of participants and their affiliations appears at the end of the paper. *e-mail: korab@iki.rssi.ru

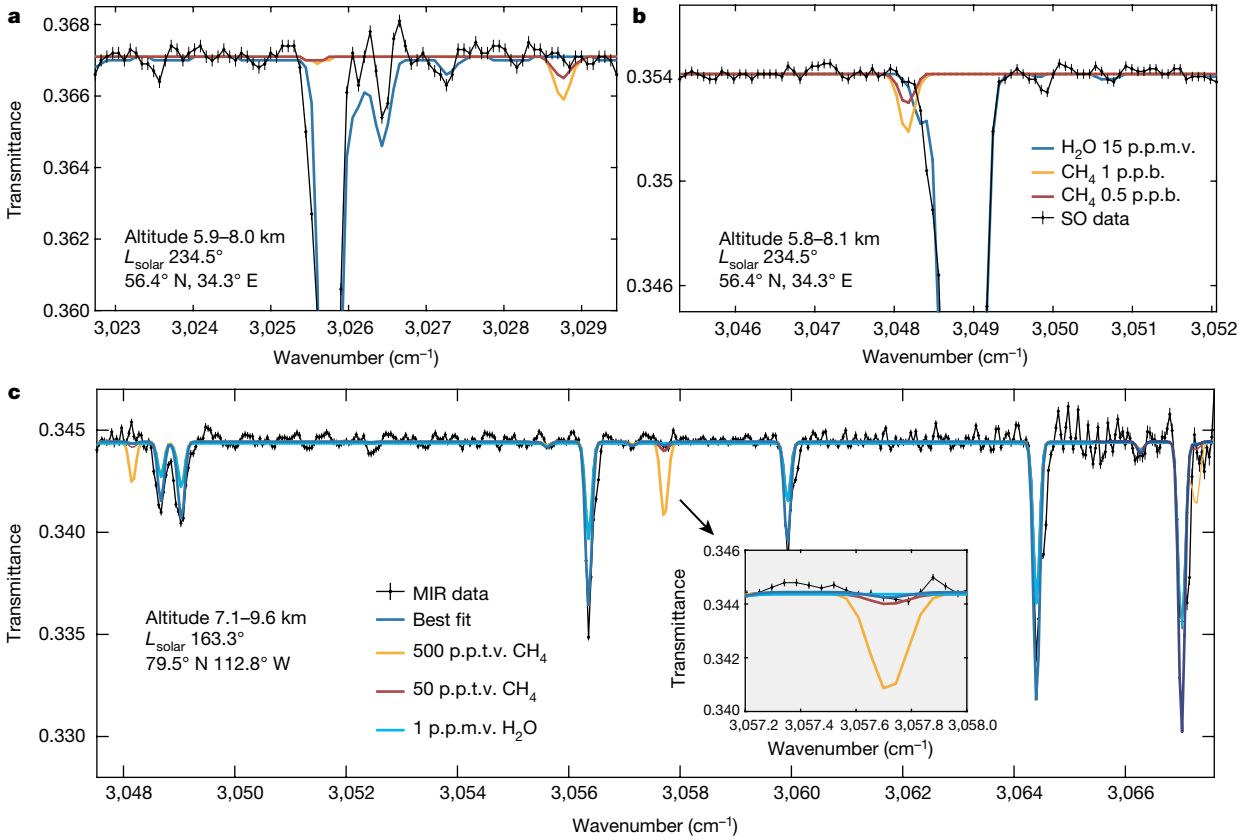

Fig. 2 | TGO spectra encompassing the spectral range with multiple methane R-branch features. a, **b**, Examples of spectra obtained by the NOMAD SO channel in two different ranges. The measurements are plotted together with synthetic models of CH_4 and of water vapour absorption. **c**, Similar results obtained by ACS MIR before the dust storm. The ACS spectrum includes the same methane feature as in **b** (3,048.2 cm^{-1}), and two stronger isolated features. The inset in **c** shows in more detail one of the strongest methane features, allowing us to constrain the methane content below a few tens of parts per trillion by volume. Measured spectra show 1σ instrument noise. The tangent altitudes above the areoid are indicated.

trace gases using solar occultations, a technique in which the spacecraft instruments observe the atmospheric absorption spectrum of sunlight during sunsets and sunrises[17]. Solar occultations provide very high sensitivity for trace-gas concentration measurements because: (1) the Sun's brightness results in very high signal-to-noise ratio (SNR) spectra; and (2) the atmospheric optical path length in occultation viewing geometry is up to ten times longer than that achieved when observing the planet's surface. Two instrument suites onboard TGO were designed to perform such measurements: ACS (the Atmospheric Chemistry Suite)[18] and NOMAD (Nadir and Occultation for MArs Discovery)[19]. Both ACS and NOMAD cover the 3.3-μm spectral range, which includes the strongest fundamental absorption bands for hydrocarbons such as CH_4, in particular the ν_3 asymmetric stretching band on which all the previous detections were made. TGO started its science operations in April 2018, with the first occultation taking place on 21 April 2018. From June until August 2018 a global-scale dust storm (GDS) reduced the transparency of the atmosphere (see ref. [20]), while high northern polar latitudes remained suitable for sensitive soundings. A map of measurements by the most sensitive channels of ACS and NOMAD in the CH_4 range is shown in Fig. 1.

When staring at the solar disk outside the atmosphere, the SNR for the ACS mid-infrared (MIR) channel reaches 10,000 (one detector line, 2-s integration time, 2.5-km vertical sampling rate), and for the NOMAD solar occultation (SO) channel SNR reaches about 2,000 (one spectrum, 48-ms integration time, 1-km sampling rate). During a solar occultation, the trace-gas detection sensitivity increases as the line of sight progressively samples closer to the surface, thereby intersecting a larger air mass. At the same time, sensitivity suffers from the increasing presence of dust and clouds, which can drastically reduce the intensity of light reaching the instrument. The atmospheric aerosol loading has previously been shown to have a negative effect on the retrieval accuracy at lower altitudes[18]. The optimum sensitivity is thus achieved at the lowest altitude where the atmosphere is still transparent enough, typically between 5 km and 25 km, corresponding to an atmospheric transmission of 0.2 to 0.5. Figure 2 shows examples of spectra acquired at an altitude close to the optimal one. No methane absorption lines are apparent, whereas we can accurately measure the faint H_2O lines within the range, which, at very low water content, have an absorption depth comparable to a 1 p.p.b.v. CH_4 absorption (Fig. 2c). The corresponding profiles for H_2O (see Methods), are characterized by an unprecedented accuracy compared to previous profiling[20,21].

On the basis of the noise level, CH_4 absorption integrated over the line of sight can be tentatively fitted along with absorption of CO_2 while taking into account the instrument spectral resolution (see Methods). In this way, an estimation of methane detection limits, converted into volume mixing ratios, for the full dataset acquired by ACS and NOMAD was made. Figure 3 illustrates the detection limits for the ensemble of observations performed by both instruments. The gradual increase in upper limits observed after the onset of the planetary dust event (GDS) (indicated by a light grey bar) is a direct consequence of dust forcing detections to occur progressively above an altitudee of 30 km, that is, above the theoretically optimal altitude (detection-wise) usually found between 15 km and 25 km. A few profiles, measured in cleaner northern conditions, were able to achieve the most precise detection limits of 0.012 p.p.b.v. down to an altitude of about 3 km (see Fig. 3).

This non-detection of methane by TGO and its associated upper limits are in contradiction with the background levels of methane of 0.41 p.p.b.v. measured in situ by the Curiosity rover at the same season[4] in previous years. As discussed above, TGO is able to detect

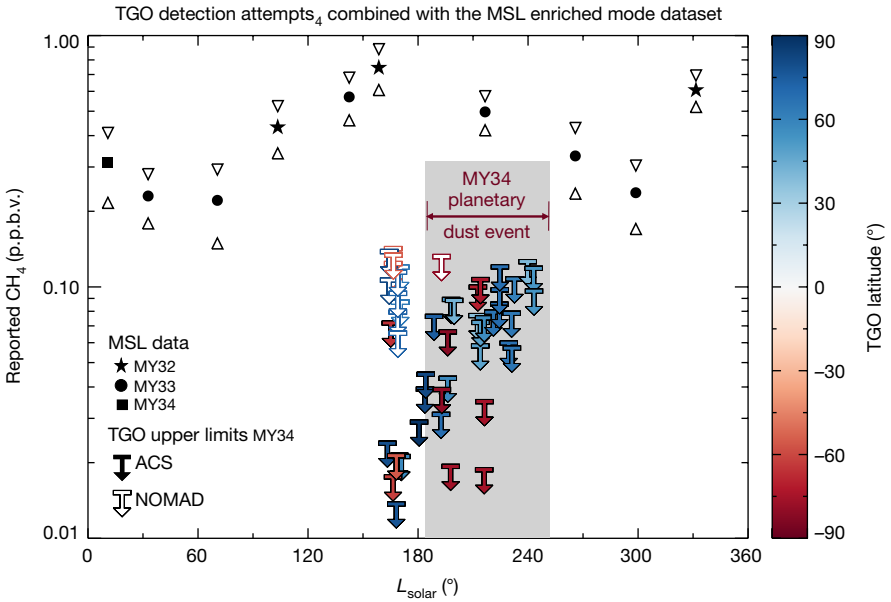

Fig. 3 | TGO detection attempts combined with the MSL enriched-mode dataset[4]. Upper limits for CH_4 (95% confidence limit) obtained by TGO (ACS and NOMAD) are compared to seasonally variable background methane as measured by SAM-TLS on Curiosity during three Martian years (MY32, MY33 and MY34). The colour scale gives the latitude of the TGO sampling. The TGO dataset has been filtered to retain only the most precise upper limits below a threshold of 0.15 p.p.b.v., encompassing values down to 0.012 p.p.b.v. The gradual increase in upper limits is associated with the onset of the planetary dust event (light grey shading).

concentrations at least ten times lower than 0.4 p.p.b.v. In fact, a simple comparison of the theoretical sensitivity of the solar occultation method with the TLS instrument method shows that TGO should be more sensitive than what can be achieved with the TLS, even when the measurements are performed using the TLS enrichment mode (see Methods).

We wondered whether the factor-of-ten difference between the MSL measurements and the TGO upper limits could result from spatial variations in the methane mixing ratios. MSL measurements were obtained at the bottom of the Gale crater near the equator, whereas the best TGO measurements were achieved in the near-polar latitudes and a few kilometres above the surface. However, it is difficult to understand why the Martian atmosphere would permit such a spatial differentiation of concentrations. On Mars, the daytime atmospheric boundary layer is characterized by intense convective motions, which mix any trace gas such as methane efficiently on a daily basis from the surface up to the top of the convective boundary layer, usually 6 km to 10 km high. From there the global wind circulation transports trace gases horizontally[6,22] and vertically around the planet. Global uniform mixing of methane occurs on a scale of 2 to 3 months[6,8,23]. Even in the extremely unlikely case in which the Gale crater constitutes the sole source of methane on Mars (note that the Gale crater and surrounding areas along the Martian dichotomy host geological features from which methane could be released[13]), MSL measurements still remain in disagreement with the detection limits derived from TGO measurements. Indeed, considering only the background concentration of 0.41 p.p.b.v., we assume that the Gale crater is uniformly and constantly filled with CH_4 up to its lowest rim (at around 2 km above areoid) and that a characteristic mixing time of one sol (ref. [4]) is the typical time for air to leave the crater. The Gale crater emission would lead CH_4 to accumulate globally over one Martian year at a level of around 2 parts per trillion by volume (p.p.t.v.). This implies that such a background emission from Gale crater could only have been going on for at most 24 Martian years (or 44 Earth years) before the detection limits reported here would have been reached. Taking into account the p.p.b.v. spikes of CH_4 concentration reported by MSL, this 24-year timeframe would be even shorter. This is unrealistic. To maintain a level of methane ten times higher than elsewhere, the Gale crater should not only be the unique source, it should also prevent its air mass from exchange with the global atmosphere. Interestingly, mesoscale model simulations have shown that the depth of the boundary layer in Gale crater is very much lowered[24] owing to the crater's size and depth. Even if this would tend to keep the methane within the crater, the same simulation[24,25] shows that the slope winds on the side of the crater and the induced updraft above the rims are so intense that methane should be efficiently injected into the atmosphere at an altitude of 10 km. We therefore cannot consider the Gale crater to be an isolated crater (see Methods for additional information).

To reconcile the lack of CH_4 detection in the TGO data and the positive CH_4 detection at the surface by the Curiosity rover, we must invoke a mechanism that is able to fully eradicate methane in the lower atmosphere at a rate approximately a thousand times faster than the rate predicted by the conventional chemistry. However, existing conventional models not only describe the chemistry of methane on Earth very well but also reproduce satisfactorily on Mars species that are sensitive to the oxidizing capacity of the atmosphere, such as hydrogen peroxide[26], ozone[27], and carbon monoxide[28]. Unless a mechanism is discovered that can rapidly destroy or sequester methane and is compatible with our wide quantitative understanding of Mars photochemistry, all the methane detections reported to date appear to be inconsistent with the present TGO measurements.

Online content

Any methods, additional references, Nature Research reporting summaries, source data, statements of data availability and associated accession codes are available at https://doi.org/10.1038/s41586-019-1096-4.

Received: 18 November 2018; Accepted: 14 March 2019;
Published online 10 April 2019.

1. Yung, Y. L. et al. Methane on Mars and habitability: challenges and responses. *Astrobiology* **18**, https://doi.org/10.1089/ast.2018.1917 (2018).
2. Mumma, M. J. et al. Strong release of methane on Mars in northern summer 2003. *Science* **323**, 1041–1045 (2009).
3. Webster, C. R. et al. Mars methane detection and variability at Gale crater. *Science* **347**, 415–417 (2015).
4. Webster, C. R. et al. Background levels of methane in Mars' atmosphere show strong seasonal variations. *Science* **360**, 1093–1096 (2018).
5. Giuranna, M. et al. Independent confirmation of a methane spike on Mars and a source region east of Gale Crater. *Nat. Geosci.* http://www.nature.com/articles/s41561-019-0331-9 (2019).
6. Lefèvre, F. & Forget, F. Observed variations of methane on Mars unexplained by known atmospheric chemistry and physics. *Nature* **460**, 720–723 (2009).
7. Zahnle, K., Freedman, R. S. & Catling, D. C. Is there methane on Mars? *Icarus* **212**, 493–503 (2011).
8. Viscardy, S., Daerden, F. & Neary, L. Formation of layers of methane in the atmosphere of Mars after surface release. *Geophys. Res. Lett.* **43**, 1868–1875 (2016).
9. Krasnopolsky, V. A., Maillard, J. P. & Owen, T. C. Detection of methane in the Martian atmosphere: evidence for life? *Icarus* **172**, 537–547 (2004).
10. Formisano, V., Atreya, S., Encrenaz, T., Ignatiev, N. & Giuranna, M. Detection of methane in the atmosphere of Mars. *Science* **306**, 1758–1761 (2004).
11. Villanueva, G. L. et al. A sensitive search for organics (CH_4, CH_3OH, H_2CO, C_2H_6, C_2H_2, C_2H_4), hydroperoxyl (HO_2), nitrogen compounds (N_2O, NH_3, HCN) and chlorine species (HCl, CH_3Cl) on Mars using ground-based high-resolution infrared spectroscopy. *Icarus* **223**, 11–27 (2013).

12. Krasnopolsky, V. Search for methane and upper limits to ethane and SO_2 on Mars. *Icarus* **217**, 144–152 (2012).
13. Zahnle, K. Play it again, SAM. *Science* **347**, 370–371 (2015).
14. Etiope, G. & Sherwood Lollar, B. Abiotic methane on Earth. *Rev. Geophys.* **51**, 276–299 (2013).
15. Oehler, D. & Etiope, G. Methane seepage on Mars: where to look and why. *Astrobiology* **17**, 1233–1264 (2017).
16. Vago, J. et al. ESA ExoMars program: the next step in exploring Mars. *Sol. Syst. Res.* **49**, 518–528 (2015).
17. Svedhem, H. et al. The ExoMars Trace Gas Orbiter. *Space Sci. Rev.* (in the press).
18. Korablev, O. et al. The Atmospheric Chemistry Suite (ACS) of three spectrometers for the ExoMars 2016 Trace Gas Orbiter. *Space Sci. Rev.* **214**, 7 (2018).
19. Vandaele, A. C. et al. NOMAD, an integrated suite of three spectrometers for the ExoMars Trace Gas mission: technical description, science objectives and expected performance. *Space Sci. Rev.* **214**, 80 (2018).
20. Vandaele, A. C. et al. Martian dust storm impact on atmospheric water and HDO/H_2O observed by ExoMars Trace Gas Orbiter. *Nature* https://www.nature.com/articles/s41586-019-1097-3 (2019).
21. Fedorova, A. et al. Water vapor in the middle atmosphere of Mars during the 2007 global dust storm. *Icarus* **300**, 440–457 (2018).
22. Mischna, M. A., Allen, M., Richardson, M. I., Newman, C. E. & Toigo, A. D. Atmospheric modeling of Mars methane surface releases. *Planet. Space Sci.* **59**, 227–237 (2011).
23. Waugh, D. W., Toigo, A. D. & Guzewich, S. D. Age of martian air: time scales for martian atmospheric transport. *Icarus* **317**, 148–157 (2019).
24. Tyler, D. & Barnes, J. R. Convergent crater circulations on Mars: influence on the surface pressure cycle and the depth of the convective boundary layer. *Geophys. Res. Lett.* **42**, 7343–7350 (2015).
25. Vasavada, A. R. et al. Assessment of environments for Mars Science Laboratory entry, descent, and surface operations. *Space Sci. Rev.* **170**, 793–835 (2012).
26. Clancy, R. T., Sandor, B. J. & Moriarty-Schieven, G. H. A measurement of the 362 GHz absorption line of Mars atmospheric H_2O_2. *Icarus* **168**, 116–121 (2004).
27. Clancy, R. T. et al. Daily global mapping of Mars ozone column abundances with MARCI UV band imaging. *Icarus* **266**, 112–133 (2016).
28. Smith, M.D. et al. The climatology of carbon monoxide and water vapor on Mars as observed by CRISM and modeled by the GEM-Mars general circulation model. *Icarus* **301**, 117–131 (2018).

Acknowledgements ExoMars is the space mission of ESA and Roscosmos. The ACS experiment is led by IKI, the Space Research Institute in Moscow, assisted by LATMOS in France. The project acknowledges funding by Roscosmos and CNES. The science operations of ACS are funded by Roscosmos and ESA. IKI affiliates acknowledge funding under grant number 14.W03.31.0017 and contract number 0120.0 602993 (0028-2014-0004) of the Russian government. The NOMAD experiment is led by the Royal Belgian Institute for Space Aeronomy (BIRA-IASB), assisted by co-PI teams from Spain (IAA-CSIC), Italy (INAF-IAPS), and the UK (Open University). This project acknowledges funding by the Belgian Science Policy Office (BELSPO), with the financial and contractual coordination of the ESA Prodex Office (PEA 4000103401 and PEA 4000121493), by Spanish MICINN through its Plan Nacional and by European funds under grants ESP2015-65064-C2-1-P and ESP2017-87143-R (MINECO/FEDER), as well as by the UK Space Agency through grants ST/R005761/1, ST/P001262/1, ST/R001405/1, ST/S00145X/1, ST/R001367/1, ST/P001572/1 and ST/R001502/1, and the Italian Space Agency through grant 2018-2-HH.0. This work was supported by the Belgian Fonds de la Recherche Scientifique—FNRS under grant number 30442502 (ET_HOME). We are indebted to the large number of people responsible for designing, building, testing, launching, communicating to and operating the spacecraft and science instruments, whose efforts made the success of TGO possible.

Reviewer information *Nature* thanks Jonathan Lunine, John Moores, Kevin Zahnle and the other anonymous reviewer(s) for their contribution to the peer review of this work.

Author contributions O.K., A.C.V. and F.M. conceived the study, collected inputs and wrote the paper. A.A.F. calibrated the ACS data and analysed the profiles (assisted by A.T., K.S.O. and J.A.). The ACS dataset was prepared by A.T. (assisted by L.B., J.A. and Y.S.I.). A.T., A.V.G., N.I.I., A.S. and A.P. designed the ACS observations. D.A.B. analysed the ACS CO_2 data. F.M. derived the methane detection limits from ACS. I.R.T. analysed the solar occultation data and provided transmittances from the NOMAD SO channel. J.T.E. and L.T., with S.A., derived the NOMAD methane detection limits. The initial General Circulation Model fields were provided by L.N. and F.D., and J.T.E. and S.R. provided and analysed the a priori knowledge and initial General Circulation Model fields. C.D. and Y.W. were involved in UVIS calibration and the data pipeline. B.R., B.B., C.Q. and E.N. designed the NOMAD observations, helped by J.M. for the UVIS channel. L.H., S.B. and R.C. are responsible for the uplink and downlink of telemetry and science data, and the first conversion of those data. M.R.P., G.B. and J.-J.L.-M. provided support in the selection of the NOMAD observations on the basis of their scientific interest. F.F., F.L. and F.D. provided critical inputs regarding the model chemistry and circulation (assisted by J.-L.B. L.N., S.V. and G.E.). C.F.W., L.Z., H.S. and J.L.V. coordinated observations of the various instruments on TGO. All authors contributed to the preparation of the manuscript.

Competing interests The authors declare no competing interests.

Additional information
Extended data is available for this paper at https://doi.org/10.1038/s41586-019-1096-4.
Reprints and permissions information is available at http://www.nature.com/reprints.
Correspondence and requests for materials should be addressed to O.K.
Publisher's note: Springer Nature remains neutral with regard to jurisdictional claims in published maps and institutional affiliations.

The ACS and NOMAD Science Teams

Gustavo Alonso-Rodrigo[14], Francesca Altieri[8], Konstantin Anufreychik[1], Gabriele Arnold[15], Sophie Bauduin[16], David Bolsée[2], Giacomo Carrozzo[8], R. Todd Clancy[17], Edward Cloutis[18], Matteo Crismani[19], Fabiana Da Pieve[2], Emiliano D'Aversa[8], Natalia Duxbury[20], Therese Encrenaz[21], Thierry Fouchet[21], Bernd Funke[9], Didier Fussen[2], Maia Garcia-Comas[9], Jean-Claude Gérard[22], Marco Giuranna[8], Leo Gkouvelis[22], Francisco Gonzalez-Galindo[9], Davide Grassi[8], Sandrine Guerlet[4], Paul Hartogh[23], James Holmes[7], Benoît Hubert[22], Jacek Kaminski[24], Ozgur Karatekin[25], Yasumasa Kasaba[26], David Kass[27], Igor Khatuntsev[1], Armin Kleinböhl[27], Nikita Kokonkov[1], Vladimir Krasnopolsky[28,29], Ruslan Kuzmin[1,30], Gaétan Lacombe[3], Orietta Lanciano[31], Emmanuel Lellouch[21], Stephen Lewis[7], Mikhail Luginin[1], Giuliano Liuzzi[19], Manuel López-Puertas[9], Miguel López-Valverde[9], Anni Määttänen[3], Arnaud Mahieux[2], Emmanuel Marcq[3], Javier Martin-Torres[32,33], Igor Maslov[1], Alexander Medvedev[23], Ehouarn Millour[4], Boris Moshkin[1], Michael J. Mumma[19], Hiromu Nakagawa[26], Robert E. Novak[19], Fabrizio Oliva[8], Dmitry Patsaev[1], Arianna Piccialli[2], Cathy Quantin-Nataf[34], Etienne Renotte[35], Birgit Ritter[22], Alexander Rodin[29], Frédéric Schmidt[36], Nick Schneider[37], Valery Shematovich[38], Michael D. Smith[19], Nicholas A. Teanby[39], Ed Thiemann[37], Nicolas Thomas[40], Jean Vander Auwera[16], Luis Vazquez[41], Geronimo Villanueva[19], Matthieu Vincendon[42], James Whiteway[43], Valérie Wilquet[2], Michael J. Wolff[17], Paulina Wolkenberg[8], Roger Yelle[44], Roland Young[4], Ludmila Zasova[1] & Maria Paz Zorzano[32,45]

[14]Instituto Universitario de Microgravedad, Universidad Politécnica de Madrid (IDR-UPM), Madrid, Spain. [15]Deutsches Zentrum für Luft- und Raumfahrt (DLR), Institute of Planetary Research, Berlin, Germany. [16]Université Libre de Bruxelles, Brussels, Belgium. [17]Space Science Institute, Boulder, CO, USA. [18]Department of Geography, University of Winnipeg, Winnipeg, Canada. [19]NASA Goddard Space Flight Center, Greenbelt, MD, USA. [20]Moscow University, Moscow, Russia. [21]Laboratoire d'études spatiales et d'instrumentation en astrophysique (LESIA), Observatoire de Paris-Meudon, Paris, France. [22]Laboratory for Planetary and Atmospheric Physics (LPAP), University of Liège, Liège, Belgium. [23]Max Planck Institute, Göttingen, Germany. [24]Institute of Geophysics, Polish Academy of Sciences, Warsaw, Poland. [25]Royal Observatory of Belgium, Brussels, Belgium. [26]Tohoku University, Sendai, Japan. [27]Jet Propulsion Laboratory, California Institute of Technology, Pasadena, CA, USA. [28]Catholic University of America, Washington, DC, USA. [29]School of Fundamental and Applied Physics, Moscow Institute of Physics and Technology (MIPT), Moscow, Russia. [30]Vernadsky Institute, Russian Academy of Sciences (RAS), Moscow, Russia. [31]Agenzia Spaziale Italiana (ASI), Rome, Italy. [32]Luleå University of Technology, Luleå, Sweden. [33]Instituto Andaluz de Ciencias de la Tierra, Universidad de Granada, Granada, Spain. [34]Laboratoire de Géologie de Lyon, Université Claude Bernard, Lyon, France. [35]Advanced Mechanical and Optical Systems (AMOS), Liège, Belgium. [36]Geosciences Paris Sud (GEOPS), Université Paris Sud, Orsay, France. [37]Laboratory for Atmospheric and Space Physics (LASP), Boulder, CO, USA. [38]Institute of Astronomy, Russian Academy of Sciences (RAS), Moscow, Russia. [39]School of Earth Sciences, University of Bristol, Bristol, UK. [40]University of Bern, Bern, Switzerland. [41]Universidad Complutense de Madrid, Madrid, Spain. [42]Institut d'Astrophysique Spatiale (IAS), Université Paris Sud, Orsay, France. [43]Centre for Research in Earth and Space Science, York University, Toronto, Canada. [44]Lunar and Planetary Laboratory (LPL), University of Arizona, Tucson, AZ, USA. [45]Centro de Astrobiología, Instituto Nacional de Técnica Aeroespacial (CSIC/INTA), Madrid, Spain.

METHODS

ACS instrument and measurements. ACS[18] consists of three infrared channels featuring high accuracy, high resolving power, and broad spectral coverage (0.7–17 μm). The MIR channel is a high-dispersion echelle spectrometer dedicated to solar occultation measurements in the 2.3–4.5-μm range. MIR has been conceived to accomplish the most sensitive measurements of Martian trace gases, while simultaneously profiling more abundant compounds such as CO_2, H_2O and their isotopologues. ACS MIR is a crossed dispersion spectrometer that measures spectra dispersed onto a cryogenic 512 × 640 pixels CdHgTe infrared array. For each acquired frame, MIR measures ≥20 adjacent diffraction orders, covering an instantaneous spectral range of 0.15–0.3 μm. To achieve the full spectral coverage, a secondary dispersion grating can be rotated to one out of 12 distinct positions (see table 3 of ref. [17] for a description of all the grating positions). Together with two other channels, the near-infrared (NIR) and the thermal infrared Fourier transform (TIRVIM) spectrometers, ACS continuously covers the spectral range between 0.7 μm and 17 μm. The NIR and TIRVIM channels are used to observe, both in solar occultation and in nadir, water vapour (H_2O), carbon monoxide (CO) and other gases including molecular oxygen (O_2) in a fundamental state. The broad spectral range acquired enables the characterization of the key meteorological parameters, including dust and water-ice cloud column opacities. In addition, the temperature profile of the atmosphere can be retrieved from the 15-μm CO_2 band sensed by TIRVIM in nadir.

Here we used ACS MIR data obtained with the secondary grating tuned to position 12. In this range, MIR acquires frames containing 20 adjacent and partially overlapping diffraction orders (from positions 172 to 192) from 3.09 μm to 3.45 μm (Extended Data Fig. 1). The instrument point spread function can be assimilated into a Gaussian function associated with a spectral resolving power of $\lambda/\Delta\lambda > 30{,}000$, where $\Delta\lambda$ is taken as the full-width at half-maximum (FWHM) of the Gaussian, that is, about 2.36σ (where σ is the standard deviation). ACS MIR was operated in the so-called 'high sensitivity' mode, where 200 frames obtained from consecutive 6-ms integration frames are stacked together onboard. One full measurement lasts 2.1 s. Depending on orbital parameters, a profile of the atmosphere from 0 km to 200 km is measured within 3 min to 6 min. The uppermost part of the occultation corresponds to the clear-Sun observations, averaged to obtain a reference intensity spectrum $\boldsymbol{I}_{\mathrm{Sun}}$. A dark signal $\boldsymbol{I}_{\mathrm{dark}}$ (the sum of the detector dark current and of the surrounding thermal background emission) is estimated from the dark part of the occultation where the Sun is fully obscured by the solid body of Mars and is refined using dedicated observations of the open space. Because the thermal environment inside the instrument is changing slightly during the occultation session as a result of internal and solar heating, $\boldsymbol{I}_{\mathrm{Sun}}$ and $\boldsymbol{I}_{\mathrm{dark}}$ are also time-dependent. To account for the gradual sub-pixel drift of the image during the occultation, we extrapolate the trend of each pixel measured during the clear-Sun observation throughout the occultation. The methane spectral range around 3,030 cm^{-1} is free of any strong gaseous absorptions, and the atmosphere above 100 km can be considered clear from any absorptions features, increasing the accuracy of the extrapolation. Each line of the detector within each stripe represents a transmittance spectrum at a certain altitude and at a wavelength range corresponding to the displayed diffraction. The resulting frame of transmittances undergoes a projective transformation to correct the artefactual curved appearance of the stripes of each diffraction order and to make it look more horizontal and thereby maintain spectral connectivity between adjacent orders (Extended Data Fig. 1). A first-order approximation of the pixel-to-wavelength calibration is established using solar lines and is then refined using the strong absorption lines of CO_2 or H_2O.

NOMAD instrument and measurements. NOMAD[19] includes three spectroscopic channels, operating from the ultraviolet and visible range to 4.3 μm. The channel most sensitive to trace gases is the SO spectrometer, providing a spectral resolving power of $\lambda/\Delta\lambda \approx 20{,}000$ in the spectral range 2.3–4.3 μm. Within this range, NOMAD SO acquires ten separate wavelength sub-ranges to profile a variety of atmospheric species. The two other channels of NOMAD are the UVIS (the ultraviolet and visible spectrometer; 200–650 nm), and the LNO (the limb, nadir and occultation) spectrometers, which can be operated both in solar occultation and in nadir. NOMAD provides vertical profiling information for atmospheric constituents at unprecedented spatial and temporal resolution. Indeed, in solar occultation, the vertical resolution is less than 1 km for the SO and UVIS channels, with a sampling rate of 1 s (one measurement every 1 km), and occultations range from the surface to an altitude of 200 km. NOMAD also provides mapping of several constituents (aerosols/dust/clouds and O_3, H_2O, HDO, CO and other trace gases) in nadir mode with an instantaneous footprint of 0.5 × 17 km^2 (the LNO spectrometer) and 5 km^2 (the UVIS spectrometer) respectively, with a repetition rate of 30 Martian sols.

For this work, we analysed SO channel data measured between 21 April and 1 August. The SO channel measures four spectral bins in each of 5 or 6 diffraction orders per second in solar occultation mode, among which a series of specific diffraction orders were chosen (orders 133 to 136 spanning the spectral range 2,990–3,080 cm^{-1}) because methane features are located within them. To increase the sensitivity of the NOMAD SO measurements, we accumulate all the spectral measurements in each occultation from the four detector bins into 3-km vertical bins. The transmittance calibration and error calculation as described by ref. [29] is adapted to consider this accumulation. By accumulating multiple measurements we improve the SNR, by increasing the 48-ms integration time for a single detector bin to an effective integration time of 144 ms for all illuminated detector bins. By accumulating multiple measurements, we effectively increase the typical 48-ms integration time of a single measurement to an average of 500-ms integration, thereby increasing the SNR compared to the previous estimation[30].

Calculation of the methane detection limits. In attempting to detect methane we have used the ACS data from diffraction orders 180 (which contains the Q-branch of the fundamental ν_3 asymmetric stretching band of CH_4), and 182 (which contains the strongest lines among the P- and R-branches) as shown in Extended Data Fig. 1 and described in the main text. Five detector lines were stacked together to form a spectrum to be fitted. We then applied a method to retrieve vertical profiles of trace gas volume mixing ratio (vmr) as developed for Mars Express solar occultation[21,31]. First, a more accurate wavelength-to-pixel dependence is established using the most intense H_2O absorption lines and is then propagated elsewhere in the occultation, in particular where the water lines are too faint. Finally, the vmr profiles of the trace constituents are retrieved by fitting the retrieved occultation portion with a pre-computed look-up synthetic model in a three-parameter space (H_2O, CH_4 vmr, and aerosol extinction) using Rodgers' regression with additional Tikhonov regularization[32]. The synthetic spectra were computed with spectral line parameters from HITRAN 2016[33] corrected to account for the CO_2 atmosphere, as described in ref. [21]. Temperature and pressure profiles were extracted from the Mars Climate Database[34]. Aerosol extinction is assumed to have a flat spectrum within a diffraction order. The retrieved profiles of H_2O and the attempts to retrieve CH_4 for two selected occultations are shown in Extended Data Fig. 2. The H_2O profiles, even though obtained from faint lines corresponding to very dry conditions, are nevertheless characterized by a greater accuracy compared to previous H_2O profilings[21]. However, this formal retrieval shows no trace of methane. Sometimes very small methane abundances of about 20 p.p.t.v. in the R-branch (3,058 cm^{-1}) were retrieved above the 1σ level. However, this result was not confirmed by a corresponding result in the Q-branch (3,018 cm^{-1}). We conclude that these constitute false-positive detections, perhaps owing to a residual fixed pattern noise in the spectrum. The effect of the atmospheric aerosol loading on the retrieval accuracy is illustrated in the right-hand-side panels of Extended Data Fig. 2 where the 'profile' of transmittance noise is shown along with the optical slant density, as measured along the line of sight.

Given that no methane was detected within the analysed dataset, we selected a faster approach to estimate robust upper limits of CH_4 vmr for the dataset considered, covering the April to August period of 2018. The sensitivity in solar occultation is produced by the number of species molecules observed along the line of sight. We assume that no methane can be retrieved within the 1σ error bars.

Near the centre of the detector, the best SNRs are achieved at a level of ≥10,000. This very low noise level implies that the main source of errors is systematic. This is the fixed pattern noise. The part of the systematic error originating from the detector dark current non-uniformity is not fully cancelled out when divided by the solar reference $\boldsymbol{I}_{\mathrm{Sun}}$ because of the nonlinearity of the detector pixels. This noise appears as a pattern with a relative level of $\leq 10^{-3}$ exhibiting a pixel-to-pixel correlation that is remanent on consecutive spectra. In Fig. 2, the fixed pattern noise is responsible for most of the visible irregularities, while the random noise (error bars shown by hairlines) becomes visible only near the edges of the detector where the signal is weaker.

To account for both the fixed pattern and the random noise, we define the instrument noise as the standard deviation of a transmission spectrum filtered from all pixel correlation wider than 2 pixels and computed over most of the diffraction order. This calculation overestimates noise in the case of spectrally narrow gaseous absorptions (because the broader ones are filtered) whose signature leaks in the pixel-to-pixel variation. We directly inferred the line-of-sight density—the number of molecules N (in units of cm^{-2}) integrated along the line of sight—of putative methane from the line-of-sight density of CO_2, which is simultaneously measured in diffraction order 178. The CH_4 line-of-sight density is estimated separately using either the CH_4 Q-branch in order 180 (3,015–3,022 cm^{-1}) or the deepest R-branch feature that can be found in order 182 (3,057–3,060 cm^{-1}); see Fig. 2.

By considering that CH_4 can be loosely detected if the tentatively retrieved value exceeds its error bar, an upper limit on CH_4 is deduced separately for the Q and R branches by assuming it to be equivalent to the error bar found for the CH_4 line-of-sight density. A multivariate regression algorithm based on a Levenberg–Marquardt approach (the MPFIT.pro IDL routine based on MINPACK-1) was used for all retrieval attempts. This algorithm provides as an output the covariance matrix of the fitted parameters whose diagonal values correspond to the square

of the error bar of every parameter. The upper limit on CH_4 vmr is then defined as the retrieved error of the CH_4 line-of-sight density divided by the CO_2 line-of-sight density. The uncertainty on CO_2 is ignored, as it accounts for only a minor fraction of the upper limit. A correspondence between the instrument SNR and the CH_4 line-of-sight density detection limit can be theoretically established. The detection limit and the step-by-step outputs of the retrieval are shown in Extended Data Fig. 3, with the resulting upper limits versus altitude in Extended Data Fig. 4.

A similar simplified retrieval method was used to estimate the detection limit from NOMAD spectra. The forward model computes the optical column density for each spectrum separately, assuming a constant mixing ratio along the line-of-sight and using the most recent HITRAN[33] CH_4 line list with CO_2 pressure broadening coefficients. The optical depth is then convoluted to the instrument's point spread function with a FWHM of 0.15 cm^{-1} and then multiplied by the grating blaze and the acousto-optic tuneable filter (AOTF) functions. The transmittance spectra are fitted by minimizing the χ^2 value using the Levenberg–Marquardt algorithm (via the Python Scipy wrapper of MINPACKS *lmder*[35]) to determine an optimal polynomial background and CH_4 mixing ratio. The standard error of the mixing ratio is derived from the covariance matrix of the optimal fit parameters. This value can be thought of as the symmetric error bound on the mixing ratio, which can affect the transmittance within the measurement noise and should be a close approximation to the detection limit.

Comparing the sensitivity of TGO solar occultations to that of SAM TLS. The SAM laser spectrometer onboard Curiosity measures gaseous absorption using an atmospheric sample in a 16.2-m-path-length cell at ambient Mars pressure (about 8 mbar)[36]. The number of air (CO_2) molecules interacting with the laser beam (the column density) is $N \approx 2 \times 10^{20}$ cm^{-2}. The very high spectral resolution of TLS allows us to resolve the natural, pressure-broadened linewidth of two methane absorption lines of about 10^{-2} cm^{-1}. For a subset of samplings, TLS was operated in a more sensitive mode where CO_2, which constitutes 96% of the atmosphere, was progressively removed from the sample, enriching the remaining gases by a factor of 20–25. The accuracy achieved is 1–2 p.p.b.v. of methane for the direct intake, and 50–100 p.p.t.v. for the enrichment mode[3,4,36].

For solar occultation geometry, the number of CO_2 molecules along the line of sight at a slant altitude of 20 km is $N \approx 10^{24}$ cm^{-2}, increasing as the surface is approached (see Extended Data Fig. 3, upper panel). The spectral resolution, as confirmed in flight, is about 0.1 cm^{-1} for the ACS MIR channel, and about 0.15 cm^{-1} for the NOMAD SO channel. ACS and NOMAD spectra give access to multiple strong features of methane in a range around 3.3 μm. By neglecting other factors, such as noise, systematic errors, contamination and so on, that potentially affect both methods, we estimate that the TGO occultation measurements are theoretically over a thousand times more sensitive than what can be achieved with the TLS direct intakes, and over thirty times more sensitive comparing to measurements performed in the enrichment mode.

Possible reconciliation of TGO and MSL measurements. The mass of CH_4 in the Gale crater, if filled to the lowest rim, can be calculated as follows: The Gale crater diameter is 154 km and its lowest rim is 2 km high, resulting in 6.7×10^{11} kg of air or 9.3×10^{36} molecules. The amount of CH_4 corresponding to a content of 0.41 p.p.b.v. is $0.41 \times 9.3 \times 10^{27}$ molecules or 100 kg of CH_4. More accurately, using MOLA topography and General Circulation Model atmospheric profiles we obtain 30 kg of CH_4, because the Gale crater is not a perfect cylinder and the air density decreases with height.

There is no reason to consider that the ten random measurements by SAM's TLS of 0.41 p.p.b.v. on average in a two year period[4] must coincide with transient methane releases, so we assume that amount to be present at all days during the Martian year. In ref. [4], the mixing rate was estimated to be one per sol, meaning that the methane in the crater is replenished every sol. So the total mass of CH_4 emitted in Gale crater over one Martian year is 20 tons or 7.5×10^{29} molecules. The full mass of the atmospheres is 2.6×10^{16} kg, giving 2×10^{-12} or 2 p.p.t.v. of well mixed CH_4. In 24 Martian years (or 44 Earth years) this accumulates to 50 p.p.t.v., and this is from just a single source in the Gale crater. Transient enrichments of methane, observed remotely[2], and spikes detected by SAM's TLS[3] further accelerate the accumulation rate.

To make the TGO and TLS-SAM results consistent (that is, an accumulation of 50 p.p.t.v. over 300 years), the mixing inside/outside the Gale crater would have to be lower than one per sol by a factor of about 7. This large factor is not consistent with mesoscale simulations, or with the strong slope winds[24,25]. A more recent simulation[37] also shows that we should not expect the Gale crater to trap any trace gas for longer than one sol. That work[37] examined water vapour, which was largely released by sublimation of overnight surface ice, and was then mixed above 3 km (compared to MOLA, so already several kilometres above the crater's highest rim) by noon and very well mixed by 4pm local Mars time on the same day. A trace gas mixed over this height range is then rapidly transported out of the Gale crater by the afternoon upslope winds, combined with the lower branch of the Hadley Circulation (northward or southward, depending on the time of year). The majority of any methane release at 6am had left the crater by 6am the next day.

Finally, the global dust storm 2018A, affecting a subset of our measurements, could not have substantially biased the conclusions of the present study. First, we establish stringent upper limits on methane before the event, and during the event in the polar areas. Second, the fact that the H_2O_2 measured in dusty conditions is well reproduced by conventional models (despite the strong sensitivity of that species to the oxidizing capacity of the atmosphere) does not suggest the existence of any major chemical mechanism on mineral dust[26,38].

Data availability

The datasets generated by the NOMAD and ACS instruments and analysed during the current study will be available in the ESA Planetary Science Archive repository, https://archives.esac.esa.int/psa, after the six months prior access period, following the ESA Rules on Information, Data and Intellectual Property. The data used for the figures are available on request from the corresponding author.

Code availability

The computer codes used to decipher the upper limits of CH_4 are available on request from the corresponding author.

29. Trompet, L. et al. Improved algorithm for the transmittance estimation of spectra obtained with SOIR/Venus Express. *Appl. Opt.* **55**, 9275–9281 (2016).
30. Liuzzi, G. et al. Methane on Mars: new insights into the sensitivity of CH_4 with the NOMAD/ExoMars spectrometer through its first in-flight calibration. *Icarus* **321**, 671–690 (2019).
31. Maltagliati, L. et al. Annual survey of water vapor vertical distribution and water–aerosol coupling in the Martian atmosphere observed by SPICAM/MEx solar occultations. *Icarus* **223**, 942–962 (2013).
32. Rodgers, C. D. *Inverse Methods for Atmospheric Sounding* Vol. 2 (World Scientific, 2000).
33. Gordon, I. E. et al. The HITRAN2016 Molecular Spectroscopic Database. *J. Quant. Spectrosc. Radiat. Transf.* **203**, 3–69 (2017).
34. Millour, E. et al. The Mars Climate Database (MCD version 5.2). European Planetary Science Congress 2015 abstr. EPSC2015-438 http://meetingorganizer.copernicus.org/EPSC2015/EPSC2015-438.pdf (2015).
35. More, J., Garbow, B. & Hillstrom, K. *User Guide for MINPACK-1 Technical Report ANL-80-74* (Argonne National Laboratory, 1980).
36. Webster, C. R. et al. Low upper limit to methane abundance on Mars. *Science* **342**, 355–357 (2013).
37. Steele, L. J., Balme, M. R., Lewis, S. R. & Spiga, A. The water cycle and regolith–atmosphere interaction at Gale crater, Mars. *Icarus* **289**, 56–79 (2017).
38. Lefèvre, F. & Krasnopolsky, V. in *The Atmosphere and Climate of Mars (ACM2017)* (ed. Haberle, R. M.) 374–404 (Cambridge Univ. Press, 2017).

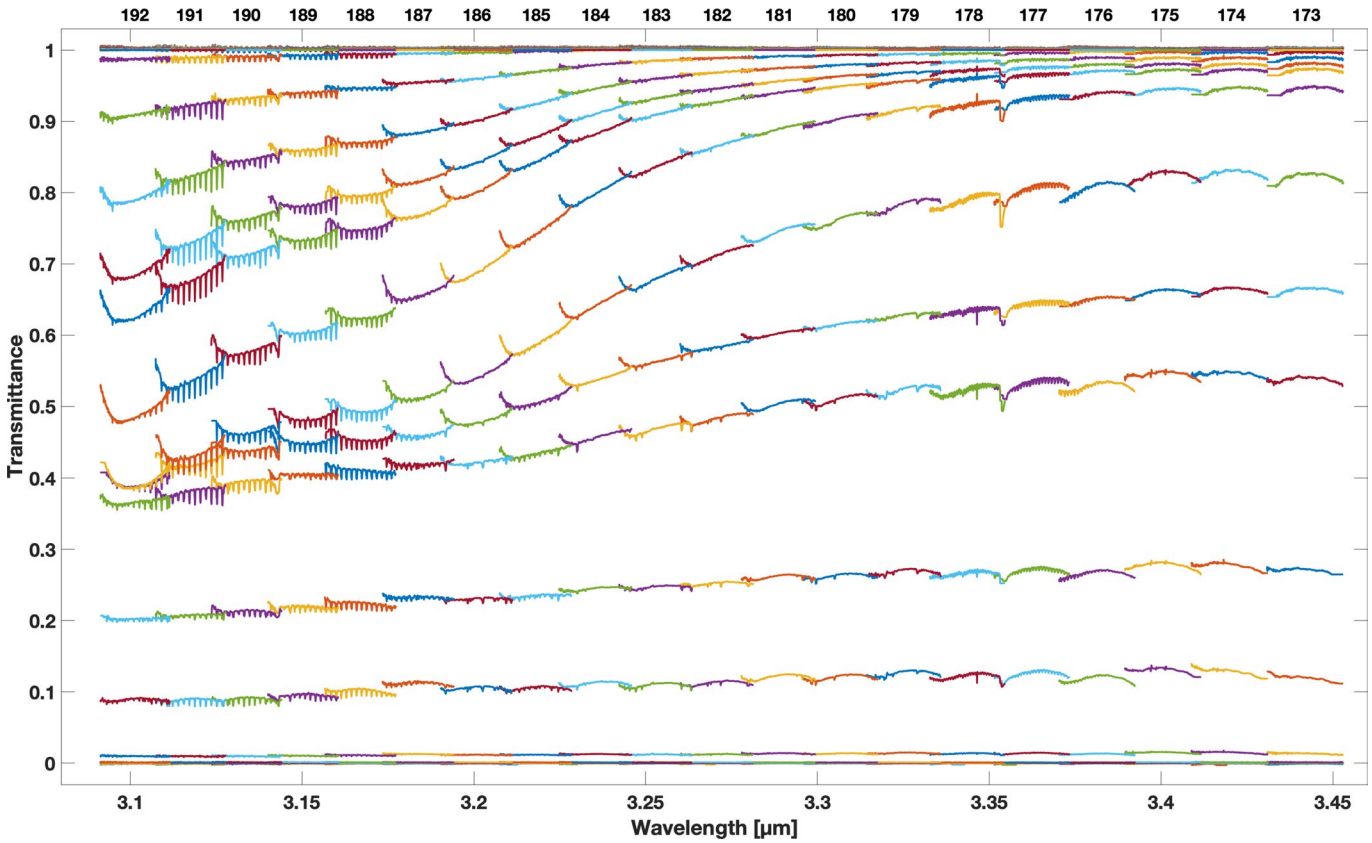

Extended Data Fig. 1 | A sequence of transmittance spectra measured with the ACS MIR channel. The spectra are for an example orbit (L_{solar} = 180.9°) obtained using the secondary grating position 12 (ref. [17]). Different diffraction orders (top axis) are denoted by the changing colour of the transmission curves, and their numbers are indicated on the upper scale. Diffraction orders used in this study are 178 (for CO_2), 180 (the CH_4 Q-branch), and 182 (the CH_4 R-branch). Enhanced extinction on the short wavelength edge of the spectra is due to H_2O ice absorption.

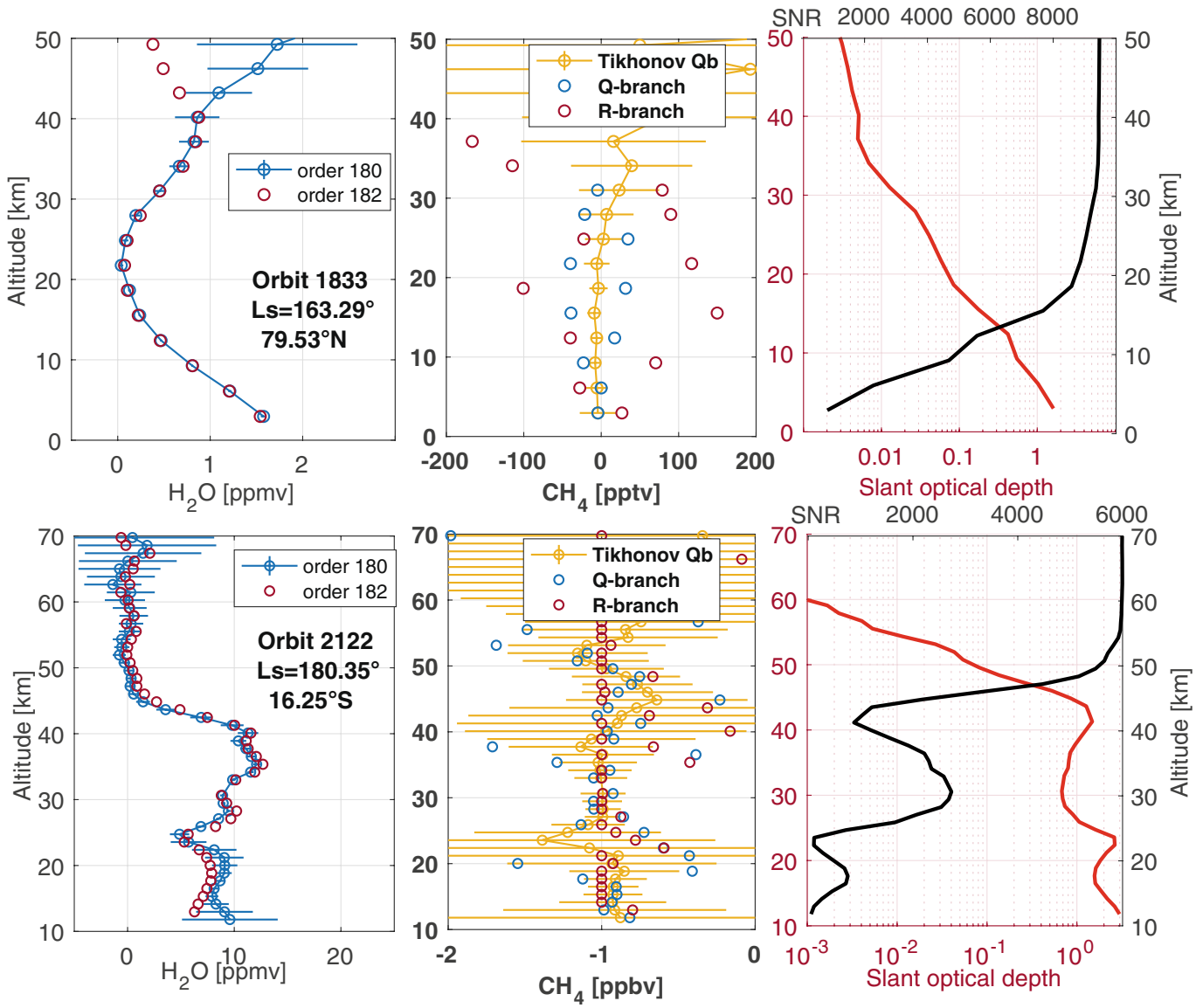

Extended Data Fig. 2 | Retrieval of trace gases from ACS MIR spectra using Rodger's regression. The spectra are for one aerosol-free polar case (upper panels), and for a more cloudy low-latitude case (lower panels). Both occultations were observed before the global dust event. Left-hand-side panels show water vapour profiles retrieved using faint H_2O absorption lines separately in diffraction orders 180 and 182. Middle panels show attempts to retrieve CH_4 in the same diffraction orders (order 180 gives access to the CH_4 Q-branch, and order 182 to the CH_4 R-branch). Curves with error bars indicate the regularized profiles (denoted as Tikhonov Qb). The error bars give the 1σ uncertainty on the retrieved parameters. To illustrate the accuracy for the individual spectra, the regularization was also turned off (scatter points). Right-hand-side panels show profiles for the optical depth on the line of sight (red), and of the SNR in the MIR spectra (black). The SNR for each spectrum was calculated over the whole diffraction order, excluding spectral intervals with gaseous features.

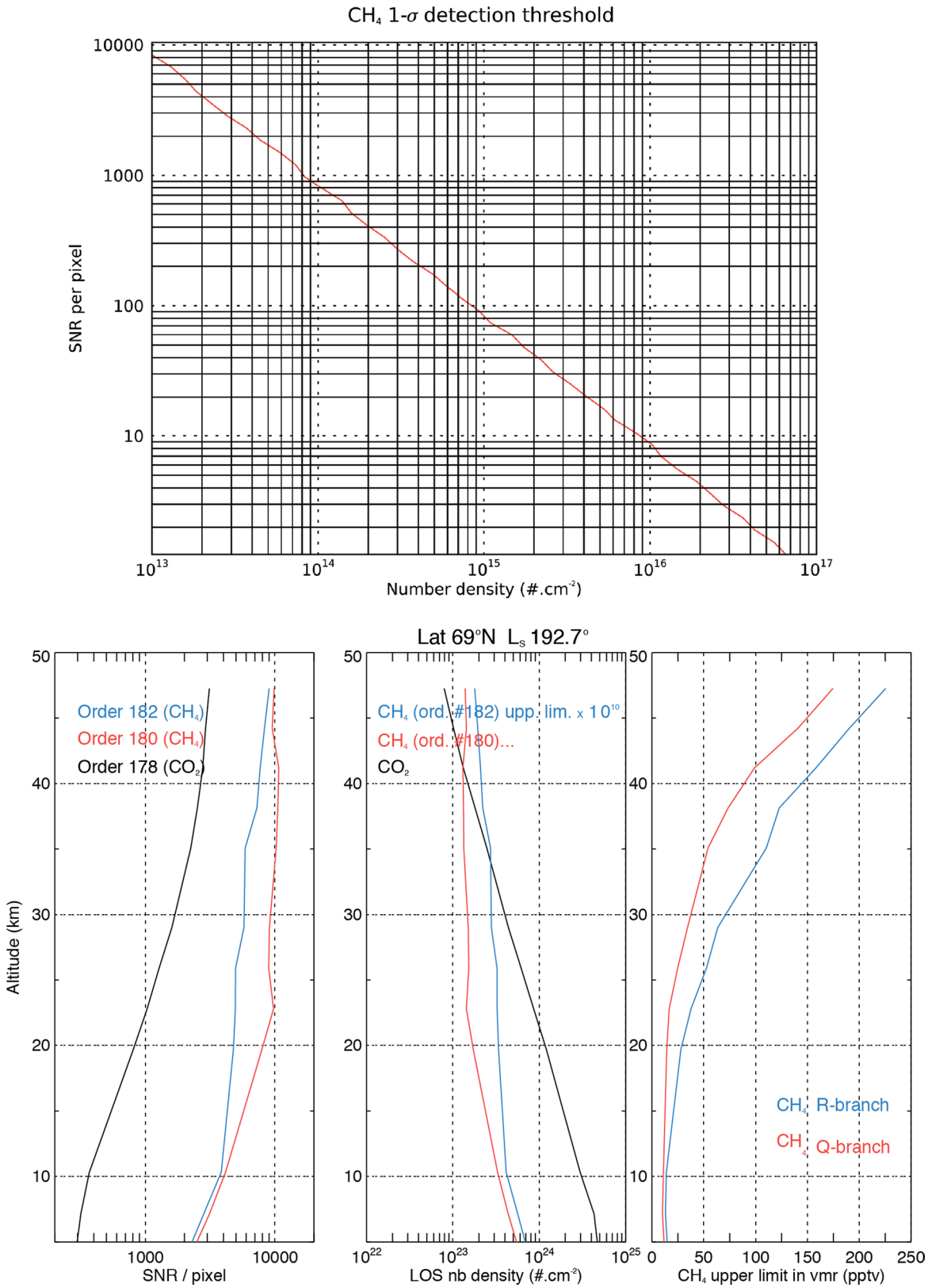

Extended Data Fig. 3 | Theoretical relation between the instrument SNR and the methane detection limit, and the step-by-step outputs of the CH_4 retrieval. Top panel, the theoretical relation between SNR per pixel and the retrieved 1σ uncertainty on the CH_4 line-of-sight density expressed in units of molecules per cm^2. At SNR >1,000 per pixel, the associated uncertainty is 10^{14} molecules per cm^2, which would yield an equivalent vmr uncertainty of 0.1 p.p.b.v. of CH_4 in the 10-km altitude range where the CO_2 density is usually around 10^{24} molecules per cm^2. Bottom panels (from left to right), altitude profiles of SNR per pixel (left), CO_2 and the error on the CH_4 line-of-sight (LOS) density in units of cm^{-2} (middle) and the resulting upper limits retrieved for CH_4 molecules (right). The displayed observation corresponds to high northern latitudes after the equinox (L_{solar} 192°; 13 June 2018). The prevailing clear conditions allowed sounding very close to the surface with high SNR, yielding optimal conditions for the retrieval of CH_4. The black, red and blue colours refer respectively to CO_2 (in order 178), CH_4 (in order 180) and CH_4 (in order 182).

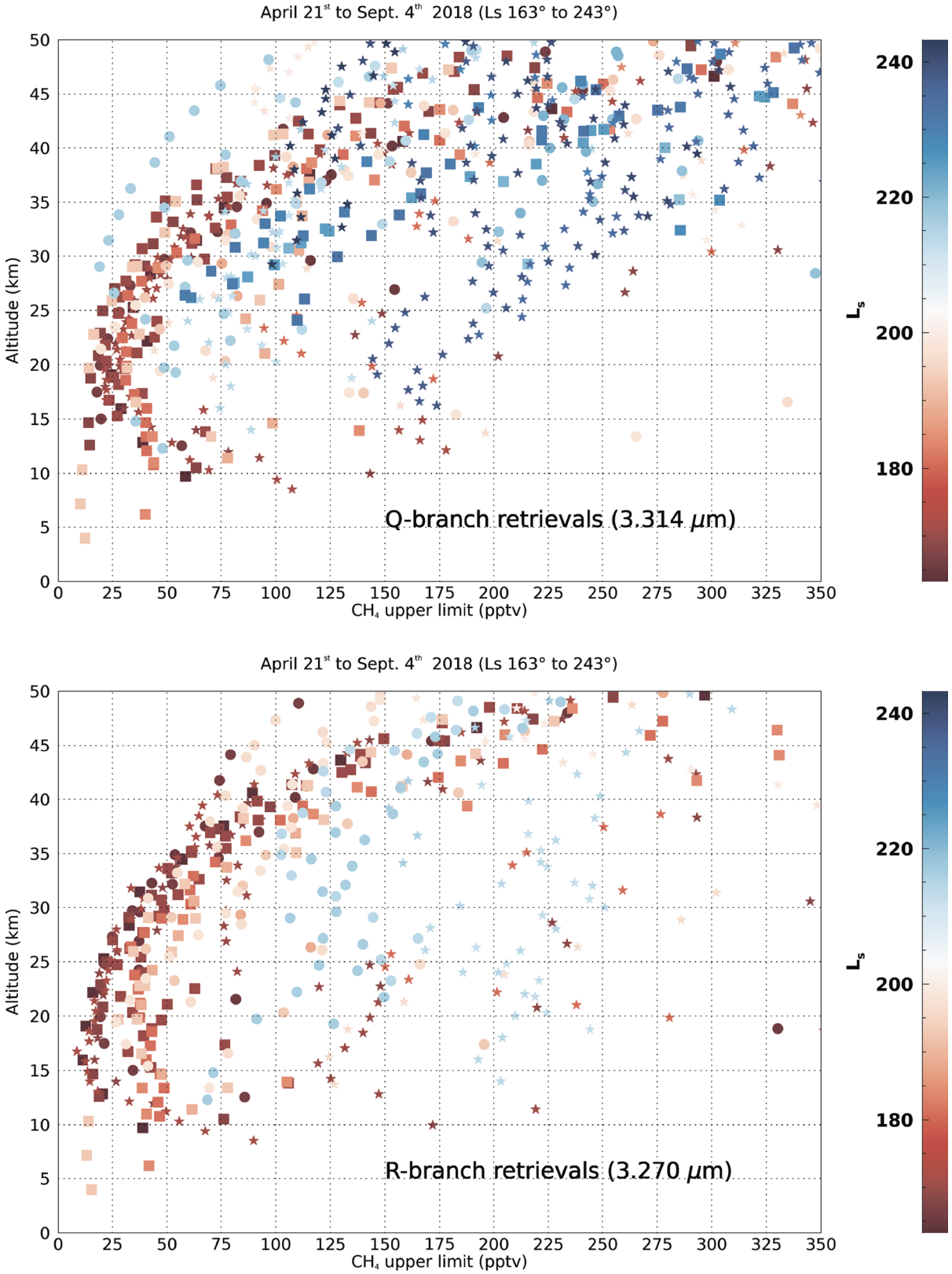

Extended Data Fig. 4 | A compilation of all the retrieved upper limits from the ACS-MIR dataset covering the period from 21 April to 4 September 2018. Top, limits from the Q-branch of CH_4 absorption; bottom, limits from the R-branch of CH_4 absorption. The colour scale denotes L_{solar}. Different symbols of similar colour designate individual profiles.